Flexible and high‐efficiency Sb2S3/solid carrier solar cell at low light intensity

Vesna Lojpur[1], Jelena Krstić[1], Zorica Kačarević‐Popović[1], Nenad Filipović[2], Ivana Lj. Validžić[1]*

[1] University in Belgrade, Vinča Institute of Nuclear Sciences, P.O. Box 522, Belgrade 11001, Serbia

[2] Institute of Technical Sciences of SASA, Knez Mihailova 35/IV, Belgrade 11000, Serbia

Abstract

Producing green and efficient energy sources is a major challenge. As a consequence, the use of photovoltaic devices for conversion of light into electricity is growing worldwide. A lot of effort had been invested to create high-efficient solar cells, but their durability, stability, flexibility and efficiency at low light intensities are still unexplored. Here, we built a flexible solar cell made of p-doped, amorphized a-undoped and n-doped Sb_2S_3 solid carrier loaded with electrolyte. Indium tin oxide glass was the working electrode, and aluminium was the counter electrode. Every (p–a–n) flexible Sb_2S_3/solid carrier layers were obtained using a cheap casting/solvent evaporation technique, from a blend consisted of chitosan, polyethylene glycol and electrolyte containing 0.5 M potassium iodide and 0.05 M iodine, and corresponding synthesized amorphized a-undoped and p and n-doped Sb_2S_3 semiconductor. Results show that flexible Sb_2S_3 solar cell possesses good stability and efficiency of about 10% at 5% sun. Overall, our findings demonstrate for the first time that flexible solar cell can be made and used for low light intensity applications.

Keywords: Solar energy materials Sb_2S_3 Solar cell Low light intensity Optics/lens

Introduction

The high demand for clean energy sources has fostered research, development and production of new solar cells (Kamat 2007). Inorganic silicon solar cells are still superior in the world market of photovoltaics with power efficiency of 15–20% (mono-crystalline device) (Bagher 2014). The main problem with silicon solar cells is the production cost. A few decades ago,

* Ivana Lj. Validžić, validzic@vinca.rs

organic photovoltaic solar cells were developed, but their expansion in research becomes higher with solar cells based on polymer thin films due to flexibility, lightweight, easy processing mechanisms and low-cost fabrications (Gunes et al. 2007). Despite many inventions and research, the best found efficiency for organic solar cells was 10% (Ahmad et al. 2018). Recently, perovskite solar cells attracted a lot of attention since their accomplished efficiency was 22% (Ansari et al. 2018). However, stability is the crucial problem of these cells that is not overcome yet, so perovskite solar cells are still only on research level.

The amount of solar energy flux that comes on Earth depends on the latitude of the geographical area. The situation is that in some parts of USA, Africa, Middle East and Australia, the annual solar irradiation exceeds 1600 kWh/m^2. Other parts of the Earth have solar irradiation far below, so it is of great importance to research and produce solar cells that can work at lower light intensities. Along with the creating and making new solar cells, efficiency at low light intensity is the main point of interest in our research.

There are many semiconductors that might be used for solar cells applications, and among them is antimony trisulphide (Sb_2S_3). Antimony trisulphide (Sb_2S_3) is important member of V–VI group semiconductors, which useful properties make it promising candidate for important applications in diverse area such as solar energy conversion due to its good photoconductivity, thermoelectric cooling technology and photoelectronics in the infrared (IR) region (Yu et al. 2006; Bao et al. 2007).

Recently, we reported solar cells that are made/based entirely on synthesized undoped and doped Sb_2S_3 semiconductor (Lojpur et al. 2017a, b; Validžic et al. 2016; Janoševic et al. 2016a, b, c). Here, we report, for the first time, flexible solar cell made of three layers, i.e. solid carriers. In first layer, Sb_2S_3 is doped with copper, in second it is undoped with amorphized Sb_2S_3, while in third layer Sb_2S_3 is doped with selenium. Indium tin oxide glass was used as a working electrode and aluminium as the counter electrode, while flexible Sb_2S_3 solid carrier was loaded with electrolyte. As far as we are aware, no similar reported cell was found in the literature.

Materials and methods

All chemicals, chitosan (Mw = 95 kDa, Sigma-Aldrich), acetic acid (Alkaloid Skoplje), polyethylene glycol (Mw = 3350 Da, Sigma-Aldrich), potassium iodide and iodine (Sigma-Aldrich) were used without further purification. Detail synthesis procedures of p-, amorphized a-undoped and n-Sb_2S_3 nanoparticles and used materials have been described previously many times (Lojpur et al. 2017a, b; Validžic et al. 2016; Janoševic et al. 2016a, b, c).

The 3% chitosan solution was obtained by dissolving chitosan in 1 M acetic acid solution at room temperature under the constant stirring for 3 h. Then, 3% aqueous solution of polyethylene glycol and potassium iodide/iodine (1.5/0.15 M) was added in order to prepare a solution in which the volume ratios of chitosan/polyethylene glycol (potassium iodide/iodine) were (5/1/1 v/v). Finally, 0.6 g of p-, amorphized a-undoped and n-doped Sb_2S_3 was put in the solution and left for constant stirring for 2 h. The obtained final solution was poured into Petri dishes and left to evaporate at room temperature. After drying in the air and in the hothouse at 40 °C, each sulphide solid carrier was placed in a hydraulic press (4 Tones) and left over night (20 h).

Thermogravimetric analysis was conducted on the Setsys Evolution (Setaram, France) in the atmosphere of synthetic air (flow rate 20 ml/min). The phase transitions were investigated on SETARAM apparatus differential scanning calorimetry (DSC) EVO 131. The X-ray diffraction (XRD) patterns were obtained on a Philips PW-1050 using CuKα radiation with a fixed 1° divergence and 0.1° receiving slits. The power output characteristics were obtained by Keithley 181 nanovoltmeter, 230 programmable voltage source and 195 A digital millimeter.

Results and discussion

The designed cell architecture is presented schematically in Fig. 1. The figure also shows an image of a thick (around 1 mm) p-doped, amorphized a-undoped and n-doped [marked with (p), (a) and (n)] flexible Sb_2S_3/solid carriers. Solid carriers are extremely flexible, and after filling with electrolyte, their softness allows good contacts in the cell.

The thermogravimetric analysis (TGA)/differential scanning calorimetry (DSC) was used to investigate the thermal characteristics/stability of obtained flexible solid carrier. These samples were recorded with the same composition but without the synthesized powders, p-doped, amorphized a-undoped and n-doped Sb_2S_3 present in the initial blend. Differential scanning calorimetry measurements of pure polyethylene glycol and solid carrier were performed, and the results are shown in Fig. 2A.

Chitosan usually does not undergo through phase transition prior to decomposition. For pure polyethylene glycol, a broad endothermic peak was observed at around 60 °C (T_m) (Sharma et al. 2016), and for three component blend, the peak was shifted to higher-temperature region, at around 95 °C. The thermogravimetric analyses for unused (A) and used (B) three component blend (Fig. 2B) showed a slight weight loss up to 50 °C. More significant weight loss for blend was noticed between 80 and 120 °C that probably come from dehydration. As far as we are aware, there are no literature reports of such blend.

Used/unused solid carrier consists of polyethylene glycol, chitosan and electrolyte potassium iodide/iodine, and X-ray diffraction patterns of starting components polyethylene glycol and chitosan as well as used and unused solid carrier without the presence of synthesized Sb_2S_3 are presented also in Fig. 2 (C and enlarged C_1). Several peaks of polyethylene glycol were observed which confirmed its crystalline nature, while for chitosan partially crystalline nature is evident for the sample. As can be seen, unused solid carrier becomes completely amorphous. This is partly due to the fact that the presence of electrolyte potassium iodide/iodine reduces crystallinity due to the salt since cation K^+ has a large radius. However, after a few months of using of the solid carrier, the electrolyte begins to crystallize in the form of potassium iodide, which is shown in Fig. 2 (C and C_1). The softness of the layers of solar cells makes it be applicable in a lot of different surfaces. The ability of adaptation to the surface is another advantage of these types of solar cells.

Typical illuminated *I–V* curves for fabricated cells under low illumination of 5% sun are shown in Fig. 3A. Two cells (3A up and down) were made to be the same. The efficiency η (in %) was calculated from the well-known relation $\eta = V_{OC}\, I_{SC}\, FF/P_{input} \times 100$, where P_{input} is the input light energy. The efficiency of the cells is 9.3 and 11.3% for 5% sun. An optical/lens system, handmade, was interposed between the lamp and the cell to prevent heating of the cell and decreases light intensity. The illuminated surfaces of the cells are 3 cm^2, while the total

surface of all the cell was 7.5 cm^2. The optic/lens system is made of two curved glass lenses (two convex surfaces in spherical form) through which circulates continuously cold water. Water pipes are integrated inlets and outlets of the lens, while at the same time, the system is completely closed and safe for work. In all our experiments, temperature effect is totally abolished by using lens/optic system with flow water layer (Lojpur et al. 2017a, b, c). Detail lens/optic system with improved photovoltaic characteristics for so far designed solar cells is given in our previous published paper (Lojpur et al. 2018). With no temperature effect and lens/optic system, we were able to obtain repeatable results with the same efficiency. Figure 3B shows a spectra of the used tungsten filament lamp, and rounded part of the spectrum represents dominant narrow energy part of the photons from 550 to 600 nm that arrives at the surface of the solar cell. The dependence of the relative transmittance of optic/lens compared to transmittance of the lamp without optic/lens on wavelengths is also shown in Fig. 3C. Obtained results indicate minimal permeability in the UV region (up to 375 nm) and almost constant value in visible and NIR regions. Using of lens/optic system with flow water layer that changes the spectrum enables the application of these solar cells in majority conditions present on Earth with low light irradiation.

The current–voltage (*I–V*) characteristics of the made cell, in the dark and illuminated by light (5% sun), as well as variation in the short-circuit current (I_{SC}) and the open-circuit voltage (V_{OC}) with time, are shown in Fig. 4. After illumination, the shift of the current–voltage (*I–V*) curves into the fourth quadrant shows that the cell worked as an electricity generator. The photovoltage and photocurrent rise and decay curves reveal that the decrease is quite a slow process.

Typical solar cell has a p–a–n diode structure, similar to amorphous silicon solar cell (Rech and Wagner 1999) where p, n and a (or i) refer to doped and intrinsic (undoped) layers. The light is entering through the p-layer, which efficiently supports hole collection in the device. A transparent conductive oxide (indium tin oxide, ITO) film contacts the diode from the front side, and, in the simplest case, a metal film serves both as rear contact and back reflector. Thick p-doped and n-doped layers build up an electric field over the intrinsic/undoped layer. Electrons and holes generated in the undoped layer are driven to the n and p-layer, respectively, by the internal electric field. It should be noted that the made cell without extra electrolyte loaded in every layer works as an electricity generator but with lower values of photocurrent and reduced efficiency (not shown).

Conclusion

In summary, for the first time we presented the designed solar cell that consists of indium tin oxide/p and n-doped and amorphized (a) undoped flexible Sb_2S_3/solid carrier loaded with electrolyte/aluminium as the counter electrode. Each of the layers was obtained by a cheap casting/solvent evaporation technique. We also presented that the cell exhibits quite high efficiency at the very low light intensity and suitable distribution which is achieved through the use of optics/lens system. It has been found that the processes in a cell are the same as in each p–a–n junction and that the presence of electrolyte facilitates and speeds up the transfer of charge through the cell.

Acknowledgements: This work is supported by the Ministry of Education, Science and Technological Development of the Republic of Serbia (Project 45005).

References

1. Ahmad Z, Najeeb MA, Shakoor RA, Al-Muhtaseb SA, Touati F (2018) Limits and possible solutions in quantum dot organic solar cells. Renew Sustain Energy Rev 82:1551–1564. https://doi.org/10.1016/j.rser.2017.07.001
2. Ansari MIH, Qurashi A, Nazeeruddin MK (2018) Frontiers, opportunities, and challenges in perovskite solar cells: a critical review. J Photochem Photobiol, C 35:1–24. https://doi.org/10.1016/j.jphotochemrev.2017.11.002
3. Bagher AM (2014) Introduction to organic solar cells. Sustain Energy 2:85–90. https://doi.org/10.12691/rse-2-3-2
4. Bao H, Cui X, Li CM, Song Q, Lu Z, Guo J (2007) Synthesis and electrical transport properties of single-crystal antimony sulfide nanowires. J Phys Chem C 111:17131–17135. https://doi.org/10.1021/jp076828q
5. Gunes S, Neugebauer H, Sariciftci NS (2007) Conjugated polymer- based organic solar cells. Chem Rev 107:1324–1338. https://doi.org/10.1021/cr050149z
6. Janošević V, Mitrić M, Bundaleski N, Rakočević Z, Validžić ILj (2016a) High-efficiency Sb_2S_3- based hybrid solar cell at low light intensity: cell made of synthesized Cu and Se-doped Sb_2S_3. Prog Photovolt Res Appl 24:704–715. https://doi.org/10.1002/pip.2724

7. Janošević V, Mitrić M, Savić J, Validžić ILj (2016b) Structural, optical, and electrical properties of applied amorphized and polycrystalline Sb_2S_3 thin films. Metall Mat Trans A 47:1460–1468. https://doi.org/10.1007/s11661-015-3282-9
8. Janošević V, Mitrić M, Janošević-Ležaić A, Validžić ILj (2016c) Weak light performance of synthesized amorphous Sb_2S_3-based hybrid solar cell. IEEE J Photovolt 6:473–479. https://doi.org/10.1109/JPHOTOV.2015.2501731
9. Kamat PV (2007) Meeting the clean energy demand: nanostructure architectures for solar energy conversion. J Phys Chem C 111:2834–2860. https://doi.org/10.1021/jp066952u
10. Lojpur V, Tasić N, Validžić ILj (2017a) Different behaviors in current–voltage measurements of undoped and doped Sb_2S_3-based solar cells. J Appl Electrochem 47:117–124. https://doi.org/10.1007/s10800-016-1025-2
11. Lojpur V, Mitrić M, Kačarević-Popović Z, Radosavljević A, Rakočević Z, Validžić ILj (2017b) The role of low light intensity: a cheap, stable, and solidly efficient amorphous Sb_2S_3 powder/hypericin composite/PVA matrix loaded with electrolyte solar cell. Environ Prog Sustain Energy 36:1507–1516. https://doi.org/10.1002/ep.12597
12. Lojpur V, Krstić J, Kačarević-Popović Z, Mitrić M, Rakočević Z, Validžić ILj (2017c) Efficient and novel Sb_2S_3 based solar cells with chitosan/poly(ethylene glycol)/electrolyte blend. Int J Energy Res. https://doi.org/10.1002/er.3899
13. Lojpur V, Mitrić M, Validžić ILj (2018) The role of low light intensity: a step towards understanding the connection between light, optic/lens and photovoltaic behavior for Sb_2S_3 thin-film solar cells. Opt Laser Technol 101:425–432. https://doi.org/10.1016/j.optlastec.2017.11.045
14. Rech B, Wagner H (1999) Potential of amorphous silicon for solar cells. Appl Phys A 69:155–167. https://doi.org/10.1007/s003390050986
15. Sharma RK, Ganesan P, Tyagi VV, Mahlia TMI (2016) Accelerated thermal cycle and chemical stability testing of polyethylene glycol (PEG) 6000 for solar thermal energy storage. Sol Energy Mater Sol Cells 147:235–239. https://doi.org/10.1016/j.solmat.2015.12.023
16. Validžić ILj, Janošević V, Mitrić M (2016) Characterization and current–voltage characteristics of solar cells based on the composite of synthesized Sb_2S_3powder with small band gap and natural dye. Environ Prog Sustain Energy 35:512–516. https://doi.org/10.1002/ep.12221

17. Yu Y, Wang RH, Chen Q, Peng LM (2006) High-quality ultralong Sb_2Se_3 and Sb_2S_3 nanoribbons on a large scale via a simple chemical route. J Phys Chem B 110:13415–13419. https://doi.org/10.1021/jp061599d

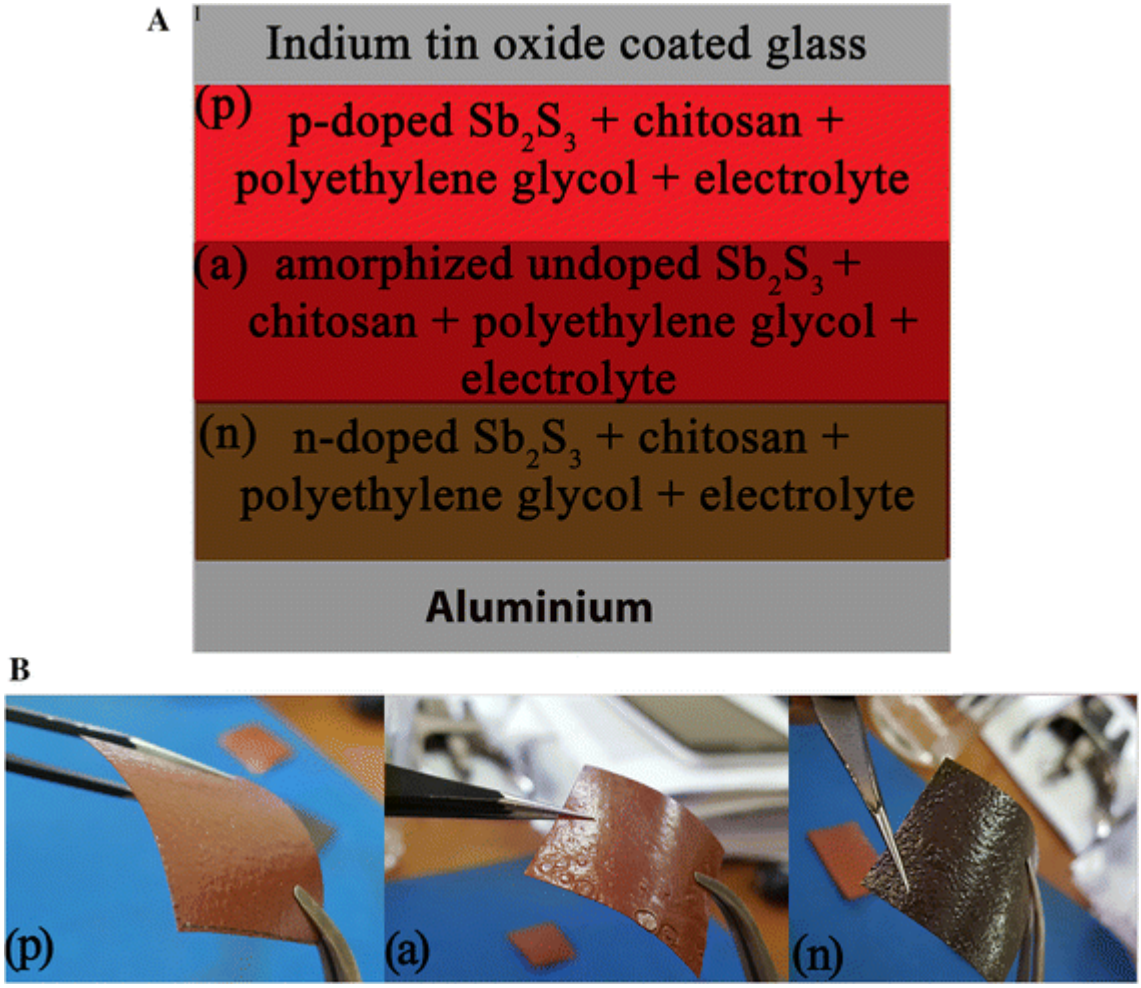

Figure 1 A schematic of designed cell with the exact composition of each of the flexible Sb_2S_3/solid layer (**A**), and photographs of designed flexible layers marked as (p), (a) and (n) (**B**). Sb_2S_3 solid layers are extremely flexible and after filing with electrolyte their softness allows good contacts in the cell

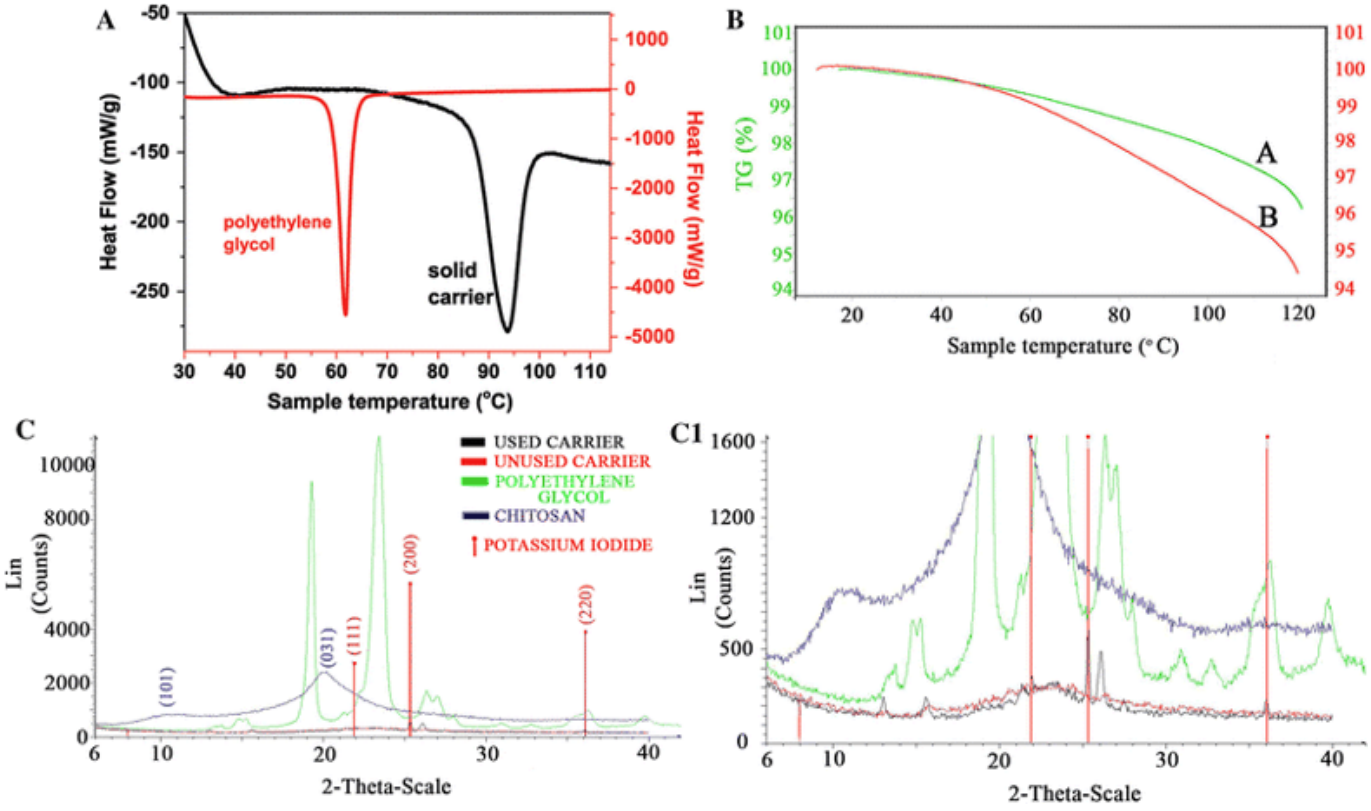

Figure 2 Differential scanning calorimetry (DSC) curves of polyethylene glycol and solid carrier with no Sb_2S_3 present (endo. down) (**A**); thermogravimetric (TG) curves of unused (A) and used (B) solid carrier (**B**); X-ray diffraction patterns for used and unused carrier, polyethylene glycol and chitosan (**C** and enlarged $\mathbf{C}_1$). Red bars indicate diffraction peaks of the potassium iodide. Corresponding planes for chitosan and potassium iodide are given, while the structure of polyethylene glycol is not resolved

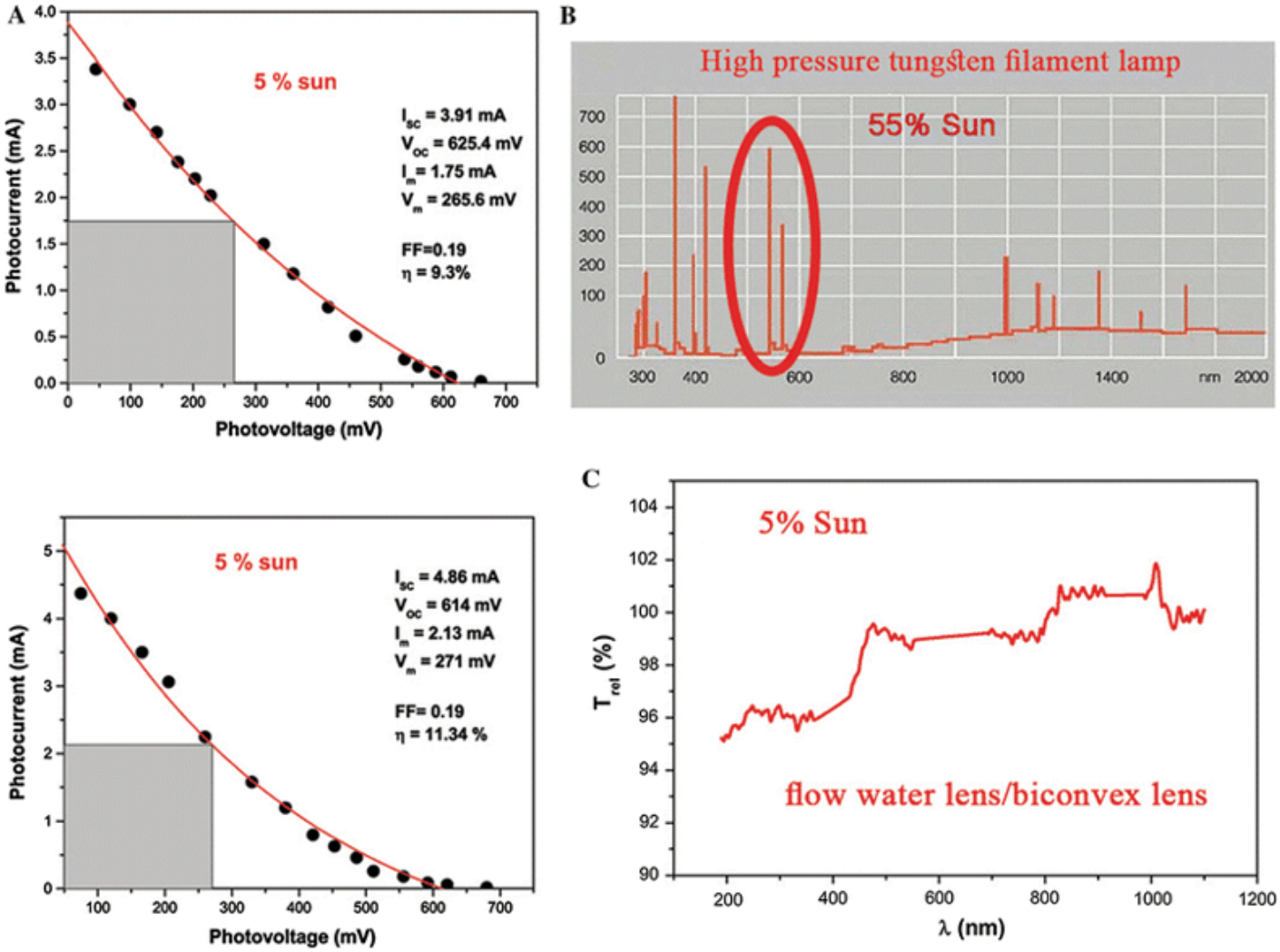

Figure 3 Illuminated current–voltage (*I–V*) curves for designed solar cell (**A**); spectra of tungsten lamp and rounded dominant part of the spectrum reaching the surface of the cell after passing through the optic/lens system (**B**); the dependence of relative transmittance of optic/lens compared to transmittance of lamp without optic/lens on wavelengths (**C**)

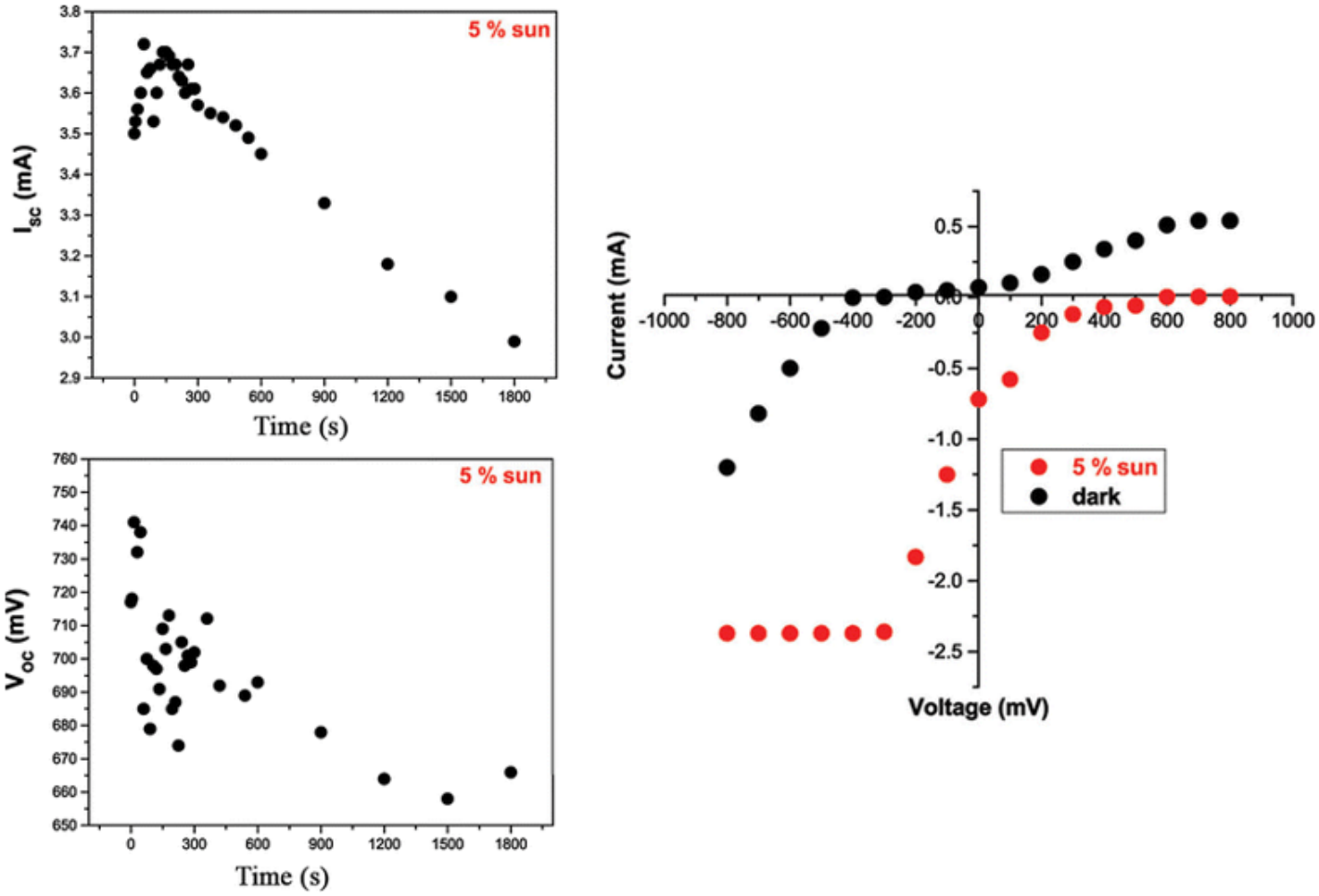

Figure 4 Variations in the short-circuit current (I_{SC}) and the open-circuit voltage (V_{OC}) with time as well as current–voltage (I–V) characteristics in dark and illuminated by the low light intensity of 5% of the sun for made solar cell. The photovoltage and photocurrent rise and decay curves reveal that the decrease is quite a slow process, while the current–voltage (I–V) curves after illumination shift into the fourth quadrant, revealing that the cell worked as an electricity generator